*15*, *25*, *26*). The structure explains the sequence of phosphorylation, dissociation, and internalization events. Serine 408 lies in the loosely structured first turn of the CD4 helix and is exposed on the surface of the complex, where it is accessible for phosphorylation (Fig. 3A). In contrast, leucines 413 and 414 are mostly buried in the hydrophobic core of the complex (Fig. 3A), so recognition of the dileucine motif by the AP-2 complex requires dissociation from Lck. The mechanism by which the complex is disrupted to unmask the internalization signal is unclear. Phosphorylation of $Ser^{408}$ is unlikely to directly disrupt the complex; comparison of HSQC spectra recorded from $^{15}$N-Lck-29 refolded with unphosphorylated or $Ser^{408}$-phosphorylated CD4 peptides confirms that this phosphorylation does not meaningfully perturb the structure of the complex (*20*). Dissociation may be induced by binding of the endocytic machinery to phosphorylated CD4, or it may involve recruitment of additional proteins that have not yet been recognized. The human immunodeficiency virus (HIV) protein Nef also induces Lck dissociation, as well as internalization and degradation of CD4, but in a manner that does not involve phosphorylation (*27*). Interestingly, Nef recognizes residues 407 to 417 of CD4, suggesting that binding of this region may be sufficient to induce Lck dissociation in spite of the $Zn^{2+}$ center (*19*).

The zinc clasp may represent an evolutionary expedient that allows reuse of a single *lck* gene product as a de facto receptor tyrosine kinase in some developmental contexts and as a nonreceptor kinase in others. Furthermore, it allows the regulated release of CD4 for internalization. The motif is unlikely to be widely employed, as even within the Src family the requisite cysteine residues are unique to Lck. These structures are examples of metal-dependent cofolding of two protein sequences. The underlying structural principle is general: Short polypeptide sequences, which are smaller and less well conserved than typical protein domains, can fold together to mediate specific, regulated protein interactions. This mechanism of interaction stands in contrast to the recognition of phosphotyrosine and proline-rich peptide motifs by the SH2 and SH3 domains of Lck, which typify modular protein interaction domains. It is unclear whether the N-terminal domain of Lck in complex with coreceptor represents a structurally isolated targeting mechanism or whether it may also affect Lck catalytic activity by impinging upon the regulatory interactions among the SH3, SH2, and kinase domains. Further investigation will be required to understand this issue and to understand precisely how the CD4-Lck complex is disrupted to allow coreceptor internalization.


**References and Notes**

1. A. Veillette, M. A. Bookman, E. M. Horak, J. B. Bolen, *Cell* **55**, 301 (1988).
2. A. S. Shaw *et al.*, *Cell* **59**, 627 (1989).
3. E. K. Barber, J. D. Dasgupta, S. F. Schlossman, J. M. Trevillyan, C. E. Rudd, *Proc. Natl. Acad. Sci. U.S.A.* **86**, 3277 (1989).
4. J. M. Turner *et al.*, *Cell* **60**, 755 (1990).
5. A. S. Shaw *et al.*, *Mol. Cell Biol.* **10**, 1853 (1990).
6. C. E. Rudd, J. M. Trevillyan, J. D. Dasgupta, L. L. Wong, S. F. Schlossman, *Proc. Natl. Acad. Sci. U.S.A.* **85**, 5190 (1988).
7. T. J. Molina *et al.*, *Nature* **357**, 161 (1992).
8. P. A. Trobridge, K. A. Forbush, S. D. Levin, *J. Immunol.* **166**, 809 (2001).
9. N. Glaichenhaus, N. Shastri, D. R. Littman, J. M. Turner, *Cell* **64**, 511 (1991).
10. T. L. Collins *et al.*, *J. Immunol.* **148**, 2159 (1992).
11. M. Iwashima, B. A. Irving, N. S. van Oers, A. C. Chan, A. Weiss, *Science* **263**, 1136 (1994).
12. R. B. Acres, P. J. Conlon, D. Y. Mochizuki, B. Gallis, *J. Biol. Chem.* **261**, 16210 (1986).
13. C. M. Weyand, J. Goronzy, C. G. Fathman, *J. Immunol.* **138**, 1351 (1987).
14. J. Shin, C. Doyle, Z. Yang, D. Kappes, J. L. Strominger, *EMBO J.* **9**, 425 (1990).
15. B. P. Sleckman *et al.*, *Proc. Natl. Acad. Sci. U.S.A.* **89**, 7566 (1992).
16. A. Pelchen-Matthews, I. Boulet, D. R. Littman, R. Fagard, M. Marsh, *J. Cell Biol.* **117**, 279 (1992).
17. R. S. Lin, C. Rodriguez, A. Veillette, H. F. Lodish, *J. Biol. Chem.* **273**, 32878 (1998).
18. M. Huse, M. J. Eck, S. C. Harrison, *J. Biol. Chem.* **273**, 18729 (1998).
19. S. Salghetti, R. Mariani, J. Skowronski, *Proc. Natl. Acad. Sci. U.S.A.* **92**, 349 (1995).
20. P. W. Kim, Z. J. Sun, S. C. Blacklow, G. Wagner, M. J. Eck, unpublished observations.
21. Materials and methods are available as supporting material on *Science* Online.
22. V. Wray *et al.*, *Biochemistry* **37**, 8527 (1998).
23. R. N. De Guzman *et al.*, *Science* **279**, 384 (1998).
24. A. Pelchen-Matthews, I. J. Parsons, M. Marsh, *J. Exp. Med.* **178**, 1209 (1993).
25. C. Pitcher, S. Honing, A. Fingerhut, K. Bowers, M. Marsh, *Mol. Biol. Cell* **10**, 677 (1999).
26. J. Shin, R. L. Dunbrack, Jr., S. Lee, J. L. Strominger, *J. Biol. Chem.* **266**, 10658 (1991).
27. J. V. Garcia, A. D. Miller, *Nature* **350**, 508 (1991).



28. We thank S. Harrison for critical comments on the manuscript. M.J.E. is a recipient of a Scholar Award from the Leukemia and Lymphoma Society. S.C.B. is a Pew Scholar in the Biomedical Sciences and an Established Investigator of the American Heart Association. This work was supported in part by NIH grants CA080942 (M.J.E.), AI37581 (G.W.), and HL61001 (S.C.B.). Atomic coordinates have been deposited in the Protein Data Bank with accession numbers 1Q68 (for CD4-Lck) and 1Q69 (for CD8-Lck).


**Supporting Online Material**

www.sciencemag.org/cgi/content/full/301/5640/1725/DC1
Materials and Methods
Figs. S1 to S4
References

14 April 2003; accepted 18 August 2003

# A Seven-Transmembrane RGS Protein That Modulates Plant Cell Proliferation


**Jin-Gui Chen,[1] Francis S. Willard,[2] Jirong Huang,[1] Jiansheng Liang,[1]* Scott A. Chasse,[3] Alan M. Jones,[1]† David P. Siderovski[2]**



**G protein–coupled receptors (GPCRs) at the cell surface activate heterotrimeric G proteins by inducing the G protein alpha (Gα) subunit to exchange guanosine diphosphate for guanosine triphosphate. Regulators of G protein signaling (RGS) proteins accelerate the deactivation of Gα subunits to reduce GPCR signaling. Here we identified an RGS protein (AtRGS1) in *Arabidopsis* that has a predicted structure similar to a GPCR as well as an RGS box with GTPase accelerating activity. Expression of AtRGS1 complemented the pheromone supersensitivity phenotype of a yeast RGS mutant, *sst2*Δ. Loss of AtRGS1 increased the activity of the *Arabidopsis* Gα subunit, resulting in increased cell elongation in hypocotyls in darkness and increased cell production in roots grown in light. These findings suggest that AtRGS1 is a critical modulator of plant cell proliferation.**


Heterotrimeric G proteins couple multiple signal transduction pathways from seven-transmembrane (7TM) GPCRs to downstream effectors in mammalian cells (*1*). RGS proteins accelerate the intrinsic guanosine triphosphatase (GTPase) activity of the Gα subunit, thus returning the heterotrimer to its basal GDP-bound state (*2*). In contrast to metazoans, the *Arabidopsis* genome contains only one canonical Gα subunit (*AtGPA1*), one G protein β (Gβ) subunit (*AtAGB1*), and two G protein γ (Gγ) subunits (*AtAGG1* and *AtAGG2*), and neither a 7TM receptor nor a cognate ligand has been identified in plants. Nonetheless, plants use heterotrimeric G protein signaling to regulate growth and development (*3*, *4*). The phenotypes of null mutants of the Gα and Gβ subunits indicate that a heterotrimeric G protein controls cell proliferation processes in *Arabidopsis* (*5*, *6*).


[1]Department of Biology, The University of North Carolina at Chapel Hill, Chapel Hill, NC 27599–3280, USA. [2]Department of Pharmacology, Lineberger Comprehensive Cancer Center, and UNC Neuroscience Center, The University of North Carolina at Chapel Hill, Chapel Hill, NC 27599–7365, USA. [3]Department of Biochemistry and Biophysics, The University of North Carolina at Chapel Hill, Chapel Hill, NC 27599–7260, USA.

*Permanent address: College of Bioscience and Biotechnology, Yangzhou University, Yangzhou 225009, People's Republic of China.

†To whom correspondence should be addressed. E-mail: alan_jones@unc.edu

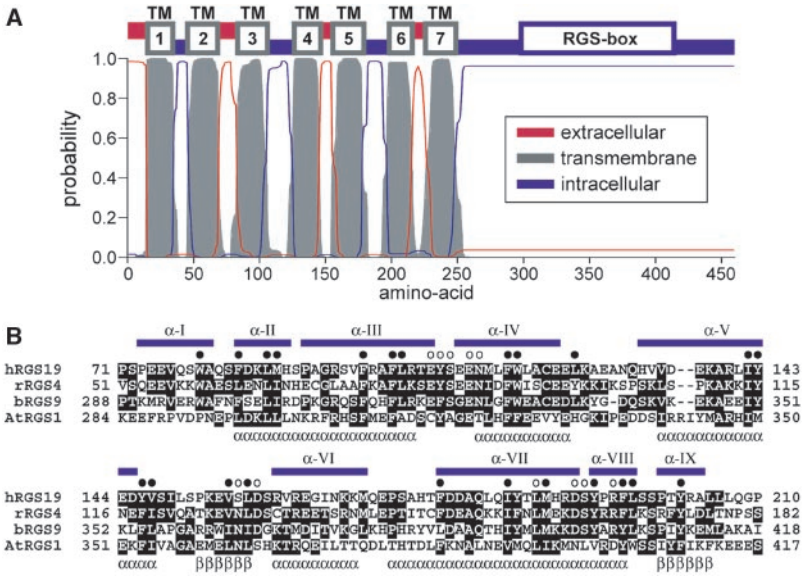


**Fig. 1.** Prediction of transmembrane regions, overall topology, and domain architecture of the AtRGS1 protein. (**A**) The probability of AtRGS1 amino acids being extracellular, transmembrane, or intracellular, as predicted using a transmembrane domain hidden Markov model (*15*), is plotted below the schematic representation of the *AtRGS1* ORF (GenPept accession number NP_189238). (**B**) Multiple sequence alignment of the RGS box regions of human hRGS19, rat rRGS4, bovine bRGS9, and *Arabidopsis* AtRGS1 proteins. Conserved amino acids identified by ClustalW (*16*) are boxed in black. The nine α helices observed within the nuclear magnetic resonance (NMR) solution structure (*17*) of hRGS19 are numbered with roman numerals and overlined in blue. Closed circles denote conserved residues forming the RGS box hydrophobic core; open circles highlight conserved residues making direct contacts with Gα in the RGS4/Gαi1 crystal structure (*10*). Predicted α helical (α) and β strand (β) secondary structure within the AtRGS1 RGS box, based on the PSI-Pred algorithm (*18*), is denoted underneath the AtRGS1 sequence. Primary sequences in the alignment are human hRGS19/GAIP (SwissProt accession number P49795), rat rRGS4 (P49799), bovine bRGS9 (O46469), and AtRGS1 (GenPept NP_189238).

A search of the *Arabidopsis* genome database for other potential components of heterotrimeric G protein signaling (*7*) revealed a single open-reading frame (ORF) of 459 amino acids (aa), hereafter called *AtRGS1*, that encodes an extended N-terminal region and a C-terminal RGS box (Fig. 1). The first 250 amino acids are predicted to form a 7TM domain with a topology reminiscent of GPCRs: an extracellular N-terminus and an intracellular C-terminus (Fig. 1A). All other known RGS proteins lack 7TM domains. The 7TM region of AtRGS1 has weak overall similarity to the metabotropic glutamate GPCR subfamily ("Family C") that also includes calcium-sensing, odorant, pheromone, and γ-aminobutyric acid type B ($GABA_B$) receptors (*8*). However, the large, ligand-binding, N-terminal ectodomain that typifies most members of this GPCR subfamily is lacking in the AtRGS1 ORF (Fig. 1A). The predicted topology of AtRGS1 places cysteine residues ($Cys^{84}$ and $Cys^{153}$) at the entry to transmembrane domain 3 (TM3) and the second extracellular loop (fig. S1), respectively, in similar positions to a common disulfide linkage found frequently in GPCRs of all subfamilies (*9*). A database search of *Arabidopsis* ORFs using the N- and C-terminal domains of AtRGS1 failed to yield homologs; thus, it appears that AtRGS1 represents the single member of this family.

The C-terminal 211 amino acids (aa 249–459) of AtRGS1, which contains the RGS box was expressed and purified from *E. coli* as a glutathione *S*-transferase (GST) fusion protein (GST-RGS1box) and was tested for its ability to bind to and accelerate the GTPase activity of AtGPA1. GST-RGS1box associated with recombinant AtGPA1 in vitro (Fig. 2A). This interaction was dependent on the addition of aluminium tetrafluoride ($AlF_4^-$), a planar ion that stabilizes Gα subunits in a transition state for GTP hydrolysis (*10*). RGS box proteins that act as GTPase-accelerating proteins (GAPs) for Gα subunits bind most avidly to the GDP-$AlF_4^-$ form of their Gα subunit targets (*10*). GST-RGS1box also accelerated the GTPase activity of AtGPA1 in a dose-dependent manner (Fig. 2, B and C). A 14-fold increase in inorganic phosphate production was observed at a threefold excess of GTP-loaded AtGPA1 over GST-RGS1box protein.

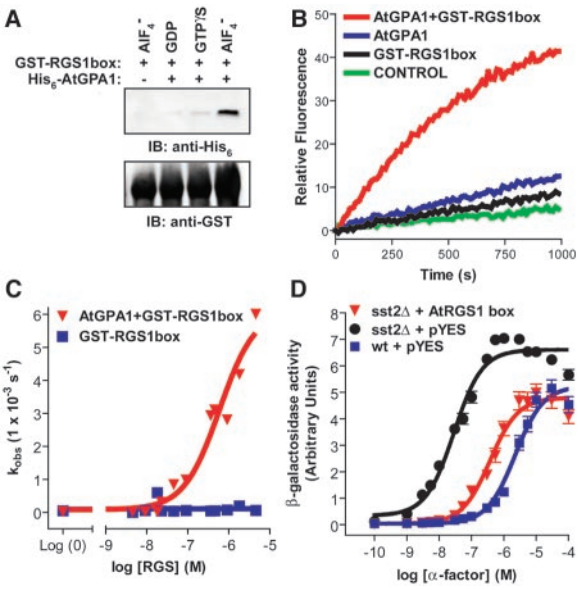


**Fig. 2.** AtRGS1 is a Gα GTPase-accelerating protein. (**A**) Guanine nucleotide dependence of the AtRGS1-AtGPA1 interaction. Purified $His_6$-AtGPA1 and GST-RGS1box (aa 249–459) proteins were incubated with GDP, GTPγS, or GDP-$AlF_4^-$ and then precipitated with glutathione agarose. Complex formation was detected by immunoblotting (IB) with specific antibodies as indicated. (**B**) GST-RGS1box accelerates the intrinsic GTPase activity of AtGPA1 in vitro. Single-turnover GTPase assays, using GTP-loaded $His_6$-AtGPA1 (575 nM) in the absence or presence of 182 nM GST-RGS1box protein, were initiated with the addition of 5 mM $MgCl_2$ at 0 s. Inorganic phosphate release was measured in real-time using fluorescent phosphate binding protein [$\lambda_{ex}$ = 425 nm, $\lambda_{em}$ = 465 nm (excitation and emission wavelengths, respectively)] and is expressed as change in fluorescence units over time (*19*). Basal level of protein-independent inorganic phosphate production is also denoted (CONTROL). (**C**) Dose-dependent AtRGS1 GAP activity. Single turnover GTPase assays were performed as in (B) using 500 nM AtGPA1 and varying concentrations of GST-RGS1box protein (0 to 4.6 μM). The apparent initial rate of phosphate production ($k_{obs}$ in $s^{-1}$), calculated from changes in fluorescence, is plotted against GST-RGS1box protein concentration. (**D**) AtRGS1 expression reverts the pheromone supersensitivity phenotype of Sst2-deficient *S. cerevisiae*. Wild-type and Sst2-null (*sst2*Δ) yeast were independently transformed with either a vector containing the C-terminal domain of AtRGS1 (AtRGS1box; aa 249–459), or empty vector (pYES), along with a pheromone-responsive *FUS1* promoter-lacZ reporter plasmid. Cells were then treated with indicated concentrations of α factor pheromone, and resultant β-galactosidase activity was measured. Median effective concentration ($EC_{50}$) values (and 95% confidence intervals) for pheromone response are as follows: wild-type yeast (squares) = 2.3 μM (1.8 to 2.8 μM); *sst2*Δ plus empty vector (circles) = 0.029 μM (0.024 to 0.035 μM); *sst2*Δ plus AtRGS1 box (inverted triangles) = 0.37 μM (0.29 to 0.49 μM).

Loss-of-function mutations to Sst2, the archetypal RGS protein of the budding yeast *Saccharomyces cerevisiae*, render haploid yeast supersensitive to pheromone signaling that is mediated by a canonical GPCR-linked signal transduction pathway (*11*). The C-terminal domain of AtRGS1 (AtRGS1box; aa 249–459) was tested for its ability to complement the

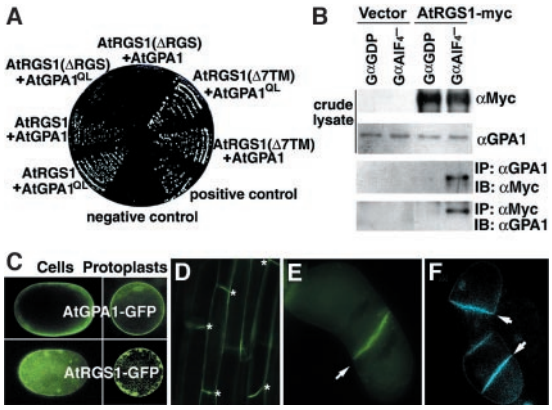


**Fig. 3.** AtRGS1 interacts with AtGPA1 in vitro and in vivo. (**A**) The C-terminus of AtRGS1 interacts with wild-type AtGPA1 and AtGPA1$^{QL}$, a constitutively active mutant form of AtGPA1, in the yeast split-ubiquitin system. Interactions between AtGPA1 (or AtGPA1$^{QL}$) and full-length AtRGS1 (aa 1–459), N-terminal 7TM (AtRGS1ΔRGS; aa 1–248), and C-terminus (AtRGS1Δ7TM; aa 249–459) were analyzed on the basis of yeast growth in selective media. The MLO1-calmodulin interaction was used as a positive control (*20*). (**B**) AtRGS1 immunoprecipitates with AtGPA1. *Arabidopsis* suspension cells were transformed with *35S::c-Myc* epitope-tagged *AtRGS1* binary vector. Total protein extracts were immunoprecipitated (IP) using antibody to c-myc (αMyc) or AtGPA1 (αGPA1) and then immunoblotted (IB) with the indicated antibody. (**C**) Both AtRGS1 and AtGPA1 localize at the plasma membrane. *35S::AtRGS1-GFP* and *35S::AtGPA1-GFP* binary constructs were transformed separately into *Arabidopsis* suspension cells. GFP was visualized by fluorescence microscopy in intact cells and protoplasts. (**D**) AtRGS1 is localized to the plasma membrane of cortical cells in the differentiated zone of *Arabidopsis* roots. Asterisks indicate the positions of apical and basal membranes. The picture was taken from the differentiation zone of a root of a 5-day-old *Arabidopsis* seedling transformed with *35S::AtRGS1-GFP*. (**E**) AtRGS1-GFP and (**F**) AtGPA1-CFP accumulate at the nascent cell plate in dividing *Arabidopsis* cells. Arrows indicate the nascent cell plate. Cells were taken from a population of suspension cells transformed with *35S::AtRGS1-GFP* or *35S::AtGPA1-CFP* binary vector 4 days after subculture.

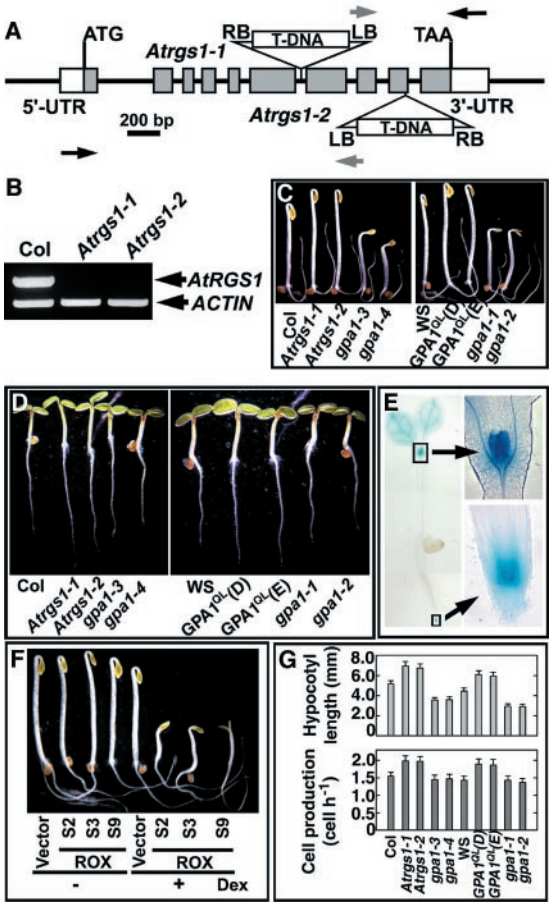


**Fig. 4.** AtRGS1 modulates cell proliferation in *Arabidopsis*. (**A**) Transferred DNA (T-DNA) insertion sites in *AtRGS1*. LB, T-DNA left border; RB, T-DNA right border. Gray boxes represent exons. The T-DNA insert is not drawn to scale. The gray arrows at LB indicate the T-DNA left border primer, and the black arrows indicate the *AtRGS1* specific primers used for mutant isolation. (**B**) Reverse transcription polymerase chain reaction (RT-PCR) analysis for *AtRGS1* transcript. The *AtRGS1* transcript was present in total RNA from wild-type *Arabidopsis* but absent in the *Atrgs1-1* and *Atrgs1-2* mutants. As a control, actin primers that amplify a 901 base pair product were added together with *AtRGS1* primers in each PCR reaction. (**C**) *AtRGS1* null allele phenotypes of 2-day-old, dark-grown seedlings. *Atrgs1-1*, *Atrgs1-2*, and null alleles of *AtGPA1* (*gpa1-3* and *gpa1-4*) are in Columbia (Col) ecotype background. Null alleles of *AtGPA1*, *gpa1-1*, and *gpa1-2*, and the transgenic lines overexpressing a constitutively active form of AtGPA1 [AtGPA1$^{QL}$ (D) and (E)] are in the Wassilewskija (WS) ecotype background. The null alleles of *AtRGS1* had the same number of epidermal cells in the hypocotyl as wild-type seedlings (fig. S3). (**D**) *AtRGS1* null allele phenotypes of 3-day-old, light-grown seedlings. (**E**) *AtRGS1::GUS* expression in light-grown *Arabidopsis* seedlings. The regions of shoot and root meristems are indicated with arrows. (**F**) Independent transgenic lines (designated ROX lines S2, S3, and S9) overexpressing *AtRGS1* driven by a dexamethasone (Dex)-inducible promoter produce a similar phenotype as the loss of *AtGPA1*. Shown here are 2-day-old, dark-grown seedlings. Plants transformed with empty pTA7002 vector were controls. Dex was applied at 0.5 μM. (**G**) Null mutants of *AtRGS1* have increased cell elongation in hypocotyls grown in darkness and increased cell production in roots grown in light. The hypocotyl lengths were taken from 2-day-old, dark-grown seedlings. The cell production in roots was measured using 5-day-old, light-grown seedlings and calculated as the rate of root growth divided by the average cortex cell length.

supersensitivity phenotype of the yeast Sst2 deletion mutant, *sst2*Δ. As observed with some mammalian RGS proteins, expression of AtRGS1 box partially restored the normal dose-response curve for α factor pheromone induction of β-galactosidase reporter gene expression placed under the control of a pheromone pathway-specific promoter (pFUS1-lacZ) (*11*), suggesting that the C-terminal domain of AtRGS1 exerts GAP activity on the yeast Gα subunit Gpa1. In addition, halo assays of pheromone-induced lethal arrest also revealed that expression of this domain can attenuate the pheromone supersensitivity of haploid *sst2*Δ yeast (*7*) (fig. S2).

Interaction between full-length AtRGS1 and AtGPA1 was shown by complementation of split ubiquitin domain fusions in yeast (*12*). The isolated AtRGS1 C-terminus [AtRGS1(Δ7TM); aa 249–459], as well as the full-length AtRGS1, interacted with both a constitutively active, GTPase-deficient form [Gln$^{222}$ → Leu$^{222}$ (Q222L)] of AtGPA1 (AtGPA1$^{QL}$) and wild-type AtGPA1 (Fig. 3A). However, the N-terminal 7TM domain of AtRGS1 [AtRGS1(ΔRGS); aa 1–248] did not interact with AtGPA1 in this assay. Full-length AtRGS1 fused to a c-myc epitope tag (AtRGS1-myc) was immunoprecipitated from *Arabidopsis* cell lysates with antiserum to AtGPA1, preferentially in the presence of $AlF_4^-$ (Fig. 3B). In the reciprocal experiment, AtGPA1 immunoprecipitated with antibody to myc, also preferentially in the presence of $AlF_4^-$. These results indicate that the full-length AtRGS1 protein interacts with endogenous AtGPA1 preferentially in the transition-state mimetic form and, thus, has the property of an RGS protein in vivo.

Expression of AtRGS1 and AtGPA1 as fusions with green fluorescent protein (AtRGS1-GFP and AtGPA1-GFP) showed localization of both proteins to the plasma membranes of postmitotic cells in culture (Fig. 3C). Plasma membrane localization of AtRGS1-GFP was maintained in fully differentiated, postmitotic cells in the intact root (Fig. 3D). In dividing *Arabidopsis* cells, both proteins accumulated at the nascent cell plate (Fig. 3, E and F), suggesting a role in cytokinesis.

Null alleles of *AtGPA1* have reduced proliferation of some cell types throughout development (*5*, *6*). Therefore, we expected that if AtRGS1 is a negative regulator of AtGPA1, null mutants of *AtRGS1* (*Atrgs1-1*, *Atrgs1-2*) would exhibit increased proliferation of some cell types, and *AtRGS1* should be expressed in some or all sites of stem cell proliferation. An *AtRGS1::GUS* transcriptional fusion transgene was predominantly expressed in shoot and root apical meristems where *AtGPA1* is also expressed (*13*) (Fig. 4E). *Atrgs1* null mutant seedlings (Fig. 4, A and B) had longer hypocotyls in the dark as a result of increased cell elongation (Fig. 4C; fig. S3). In contrast, null alleles of *AtGPA1* (*Atgpa1-1* → *-4*) (*5*, *14*) caused shorter hypocotyls, although this phenotype is due to

fewer cells (*5*). Expression of the constitutively active AtGPA1$^{QL}$ increased etiolated hypocotyl length due to increased cell elongation, similar to the *Atrgs1*-null mutants (Fig. 4, C and G).

In light-grown seedlings, both null mutants of *AtRGS1* and lines overexpressing AtGPA1$^{QL}$ produced longer primary roots compared with wild-type *Arabidopsis* or null mutants of *AtGPA1* (Fig. 4D). This increased root growth phenotype resulted from increased cell production in root meristems (Fig. 4G). These data suggest that increased activity of AtGPA1, either by expression of constitutively active AtGPA1$^{QL}$ or through loss of AtRGS1 expression, results in increased cell proliferation in the apical root meristem. Inducible overexpression of *AtRGS1* (*7*) (fig. S4) produced a similar phenotype as loss of *AtGPA1* (Fig. 4F), further suggesting that AtRGS1 antagonizes the activation of AtGPA1. In addition, some loss-of-function *gpa1* phenotypes, such as paclobutrazol and sugar sensitivity, are the opposite in the *Atrgs1* mutants, indicating a role for activated GPA1 in other signaling pathways throughout development (figs. S5 and S6).

Heterologous expression of full-length AtRGS1 protein in Sf9 insect cells has not yet provided adequate expression levels for a biochemical test of GAP activity in vitro. Nevertheless, the evidence that null mutants of AtRGS1 phenocopy the constitutively active mutant form of AtGPA1 (AtGPA1$^{QL}$), that overexpression of AtRGS1 antagonizes the activation of AtGPA1 (Fig. 4), and that full-length AtRGS1 interacts with AtGPA1 in an $AlF_4^-$-dependent manner (Fig. 3) suggests that AtRGS1 exerts GAP activity on AtGPA1 in vivo. Our results here support earlier findings that cell proliferation in plants is regulated by heterotrimeric G protein subunits and further extend those findings by showing that this regulation is cell type specific. It also reveals that cell proliferation control by the *Arabidopsis* G protein mechanistically involves either the unsequestered Gβγ subunit or the activated Gα subunit as the predominant regulatory element, depending on cell type.


**References and Notes**

1. H. E. Hamm, *J. Biol. Chem.* **273**, 669 (1998).
2. R. R. Neubig, D. P. Siderovski, *Nature Rev. Drug Discov.* **1**, 187 (2002).
3. A. M. Jones, *Curr. Opin. Plant Biol.* **5**, 402 (2002).
4. S. M. Assmann, *Plant Cell* **Suppl. 14**, S355 (2002).
5. H. Ullah *et al.*, *Science* **292**, 2066 (2001).
6. H. Ullah *et al.*, *Plant Cell* **15**, 393 (2003).
7. Materials and methods are provided as supplemental materials on *Science* Online.
8. The N-terminal 250 residues of AtRGS1 were submitted to the SMART server (http://smart.embl-heidelberg.de) for 7TM prediction and returned similarity to a Pfam model of Family C GPCRs with an expect value (E) of $2.8 \times 10^{-1}$ as described by A. Bateman *et al.* [*Nucleic Acids Res.* **30**, 276 (2002)].
9. U. Gether, *Endocrine Rev.* **21**, 90 (2000).
10. J. J. Tesmer, D. M. Berman, A. G. Gilman, S. R. Sprang, *Cell* **89**, 251 (1997).
11. H. G. Dohlman, J. Song, D. Ma, W. E. Courchesne, J. Thorner, *Mol. Biol. Cell* **16**, 5194 (1996).
12. I. Stagljar, C. Korostensky, N. Johnsson, S. te Heesen, *Proc. Natl. Acad. Sci. U.S.A.* **95**, 5187 (1998).
13. H. Huang, C. Weiss, H. Ma, *Int. J. Plant Sci.* **155**, 3 (1994).
14. A. M. Jones, J. R. Ecker, J. G. Chen, *Plant Physiol.* **131**, 1623 (2003).
15. A. Krogh, B. Larsson, G. von Heijne, E. L. L. Sonnhammer, *J. Mol. Biol.* **305**, 567 (2001).
16. J. D. Thompson, T. J. Gibson, F. Plewniak, F. Jeanmougin, D. G. Higgins, *Nucleic Acids Res.* **24**, 4876 (1997).
17. E. de Alba, L. De Vries, M. G. Farquhar, N. Tjandra, *J. Mol. Biol.* **291**, 927 (1999).
18. L. J. McGuffin, K. Bryson, D. T. Jones, *Bioinformatics* **16**, 404 (1999).
19. R. J. Kimple *et al.*, *Comb. Chem. High Throughput Screen.* **6**, 399 (2003).
20. M. C. Kim *et al.*, *Nature* **416**, 447 (2002).


21. We thank H. G. Dohlman for comments on the manuscript, R. Panstruga (Max Planck Institüt Köln), C. Koncz (Max-Planck Institüt für Züchtungsforschung-Köln), and N.-H. Chua (Rockefeller University) for materials and technical assistance. Work in A.M.J.'s lab is supported by the National Institute of General Medical Sciences (GM65989) and NSF (0209711). D.P.S. is supported by a Year 2000 Neuroscience Scholarship from the EJLB Foundation, a Burroughs-Wellcome Fund New Investigator Award in the Pharmacological Sciences, and grants from NIGMS (GM62338 and GM65533). S.C. is supported by a grant from the NIH (GM055316) to H. Dohlman. J.L. is supported, in part, by the Chinese Key National Basic Research and Development Program.


**Supporting Online Material**

www.sciencemag.org/cgi/content/full/301/5640/1728/DC1
Materials and Methods
Figs. S1 to S6

9 June 2003; accepted 31 July 2003

# Demography of Dietary Restriction and Death in *Drosophila*

**William Mair,[1] Patrick Goymer,[1,2] Scott D. Pletcher,[1]* Linda Partridge[1]†**

**Dietary restriction (DR) increases life-span in organisms from yeast to mammals, presumably by slowing the accumulation of aging-related damage. Here we show that in *Drosophila*, DR extends life-span entirely by reducing the short-term risk of death. Two days after the application of DR at any age for the first time, previously fully fed flies are no more likely to die than flies of the same age that have been subjected to long-term DR. DR of mammals may also reduce short-term risk of death, and hence DR instigated at any age could generate a full reversal of mortality.**

Dietary restriction (DR) prolongs life-span and delays the onset of many age-related declines in function (*1–4*). In *Drosophila*, DR is applied by maintenance of adult flies on a food medium that contains roughly 35% less yeast and sugar than standard laboratory medium (*2*, *5*). Both mean and maximum life-span are increased under DR conditions (*5*). Age-specific mortality is a measure of the instantaneous hazard of death for an individual at a given age. Unlike survivorship analysis, which is a cumulative measure, age-specific mortality allows independent comparisons of vulnerability to death at different ages (*6*, *7*). In *Drosophila*, chronic DR results in a delay in the onset of a detectable aging-related increase in mortality (*5*). Once the mortality increase is detected, however, it proceeds at roughly the same rate in DR and control flies (*5*).

Interventions can lower adult mortality by slowing the accumulation of the irreversible damage that is characteristic of aging (aging-related damage), by reducing short-term vulnerability to death (risk), or by some combination of the two (*8*). We can distinguish these hypotheses experimentally for DR by examining the effect of past and current nutritional conditions on age-specific mortality. This type of approach has shown that, in *Drosophila*, increased reproductive activity in males (*8*) and yeast deprivation in females (*9*) result in a higher mortality that is entirely due to an increased risk of death. In contrast, Mediterranean fruit flies (*Ceratitis capitata*) switched from sugar only to sugar and yeast food were permanently affected by their previous diet (*10*). If DR acts solely by slowing the accumulation of aging-related damage, then the onset of DR would not lead to a drop in mortality rate, because the damage would not be reversed. However, DR would result in a slower subsequent accumulation of aging-related damage and, hence, a less rapid subsequent increase in

[1]Department of Biology, University College London, Darwin Building, Gower Street, London WC1E 6BT, UK. [2]Natural Environment Research Council (NERC) Centre for Population Biology, Imperial College, London, Silwood Park Campus, Ascot, Berkshire SL5 7PY, UK.

*Present address: Department of Molecular and Human Genetics and Huffington Center on Aging, Baylor College of Medicine, Houston, TX 77030, USA.
†To whom correspondence should be addressed. E-mail: l.partridge@ucl.ac.uk